International Journal of Thermal Sciences 173 (2022) 107414

Contents lists available at ScienceDirect

International Journal of Thermal Sciences

journal homepage: www.elsevier.com/locate/ijts

Decoupling mechanisms of "avalanche" phenomenon for laser ablation of C/SiC composites in hypersonic airflow environment

Zhe Wang [a,b], Ruixing Wang [a,b,*], Hongwei Song [a,b], Te Ma [a,b], Jiangtao Wang [a,b], Wu Yuan [a,b], Chenguang Huang [b]

[a] Key Laboratory for Mechanics in Fluid-Solid Coupling Systems, Institute of Mechanics, Chinese Academy of Sciences, Beijing, 100190, China
[b] School of Engineering Sciences, University of Chinese Academy of Sciences, Beijing, 100049, China

ARTICLE INFO

Keywords:
C/SiC composite
Hypersonic airflow
Laser ablation behavior
Thermomechanical erosion
Coupled fluid-thermal-ablation analysis

ABSTRACT

When C/SiC composites subjected to high-power laser irradiation under hypersonic airflow environment, "avalanche" phenomenon was found, i.e., the ablation rate was significantly higher than that under static air environment. To reveal this phenomenon, parallel experiments of laser ablation under static air, short-time and long-time hypersonic airflow environments were carried out. Ablation models including oxidation, sublimation and erosion considering coupling effects of airflow and C/SiC composites were introduced, and a coupled fluid-thermal-ablation numerical simulation procedure was proposed and carried out. The relationship between ablation rates and aerodynamic pressure was discussed, and the contributions of different ablation mechanisms were quantitively evaluated. In hypersonic airflow environments, sublimation rate was increased due to the decreased local pressure, and erosion rate was accelerated as a result of increased pressure head at downstream area. The combined effect of augmented sublimation and accelerated erosion accounted for the main reason of "avalanche" phenomenon under hypersonic airflow.

1. Introduction

As one kind of typical ceramic matrix composites (CMCs), C/SiC composites have been widely applied in the thermal protection systems (TPS) of hypersonic vehicles. The ablation performance of the C/SiC composite is closely related to its practical service life, and has a remarkable effect on the design of hypersonic vehicle structures [1–3]. Given the advantages of the controllable and stable heat source and the non-additional chemical reaction, the high-power laser has become a new method to investigate the ablation behavior. And the laser ablation performance of thermal protection materials has become a hot research topic [4–10].

In the past decades, relevant studies mainly focused on the laser ablation behavior of C/SiC composites in the static air, and the corresponding ablation mechanisms were clearly revealed [8–10]. Researches showed that the sublimation effect was the main cause of the evolution of the ablation center due to the local low oxygen and high temperature, and oxidation reaction dominated the ablation progress in the region which at relatively low temperature. In addition, the SiO_2 layer caused by oxidized SiC prevented the further oxidization of material. However, in recent years, the impact of high-speed airflow on the laser ablation performance, which cannot be neglected for the high-speed vehicles in service, has caused extensive concern. In our recent work, we have primarily studied the laser ablation behavior of C/SiC composites subjected to tangential supersonic and hypersonic airflows through experimental research [11,12]. It was observed that the significantly accelerated ablation phenomenon occurred under the high-speed airflow. Especially for the hypersonic airflow, the mass ablation rates were augmented by 4–9 times when compared with the static air condition. We name this significantly accelerated ablation phenomenon as "avalanche" phenomenon. However, it should be noted that although the acceleration effects caused by the high-speed airflow have been observed by the experiments, the inherent mechanisms are still unclear due to the complex interaction of laser, matter and high-speed airflow. Therefore, further studies on the fully-coupled numerical analysis are needed to quantitatively reveal the accelerated ablation mechanisms for "avalanche" phenomenon.

Generally, the laser ablation behavior of C/SiC composites in high-

* Corresponding author. Key Laboratory for Mechanics in Fluid-Solid Coupling Systems, Institute of Mechanics, Chinese Academy of Sciences, Beijing, 100190, China.
E-mail address: wangruixing@imech.ac.cn (R. Wang).

https://doi.org/10.1016/j.ijthermalsci.2021.107414
Received 25 August 2021; Received in revised form 23 November 2021; Accepted 24 November 2021
Available online 2 December 2021
1290-0729/© 2021 Elsevier Masson SAS. All rights reserved.

speed airflow is a typical heat and mass transfer process with strong multi-physics coupling effects. The thermomechanical ablation models considering the action of overrunning airflow are the foundation of the coupled thermal-fluid-ablation model. Dimitrienko [13–15] established the relationships of the linear rate for different types of surface ablation (e.g., oxidization, sublimation, melting and erosion). Park [16–19] proposed the finite-rate ablation model for the calculation of the recession rate, due to various surface-gas reactions. Li [20–24] provided a series of ablation models to solve the surface ablation for charring composites, and a coupled thermal-fluid-chemical method was considered. Ren [25] developed a theoretical analysis for the mechanical erosion of carbon-base materials, which accounted for the heating, pressure, and shear forces acting on the material. Barr [26] developed a mechanical erosion model to defines the erosion rate, which was related to the surface shear stress and surface temperature. However, current research on the ablation model was concentrated for carbon matrix composites. Luan [27] proposed a multi-zone load bearing model for stressed oxidation of C/SiC, and studied the stressed oxidation lifetime for the composites in a high temperature wind tunnel. But for C/SiC composites, studies on the coupling ablation models are still rare at present. It is necessary to establish complete analysis models including sublimation, oxidation and mechanical erosion, which are applicable for the multi-field coupling environment.

Moreover, the multi-physics coupled analysis method incorporating ablation models, coupling strategy, date exchange, mesh deformation is another key issue. Many efforts have been devoted to predicting the ablation behavior of the ablative thermal protection systems for hypersonic vehicles in the reentry environment [28–32]. Martin [29] presented a material response code strongly coupled with a hypersonic flow solver to improve the solution of heat and ablation rate for hypersonic vehicles. Meng [30] proposed a coupled fluid-thermal-ablation analysis for a carbon/carbon composite leading edge in hypersonic airflow, and a mesh movement algorithm was implemented in the finite element method to achieve surface recession. Schrooyen [31] proposed a coupling algorithm, which allowed for time accurate solutions of the ablative material thermal response accounting for surface chemistry, material behavior, and surface recession. However, for the laser ablation behavior in the hypersonic airflow, the coupling action of high-power laser and high-speed airflow would lead to more complex interaction effects due to the high heating rate and large ablation deformation in the local region. Thus, a new coupling numerical analysis method should be established to reveal the laser ablation mechanism of C/SiC composite in hypersonic airflow.

The purpose of this paper is to carefully disclose the acceleration mechanisms of laser ablation behavior for C/SiC composites in the hypersonic airflow environment experimentally and numerically. The experimental research was firstly conducted to investigate the accelerated laser ablation phenomena under different environments, i.e., static air, short-time and long-time hypersonic airflow environments. Then, the coupled thermal-fluid-ablation numerical analysis model, which was validated by the experimental results, was developed to reproduce the detailed ablation process. Therefore, the interaction effects between the hypersonic airflow and the thermomechanical ablation behavior were quantitatively evaluated. By decoupling different mechanisms, the cause of "avalanche" phenomenon for laser ablation of C/SiC composites under tangential hypersonic airflow were clearly expounded.

2. Experimental research

As displayed in Fig. 1, a continuous wave laser beam was employed as a heat source to conduct the ablation tests of 2D C/SiC composites in a hypersonic free jet wind tunnel. The size of samples for ablation tests was 50 mm × 50 mm × 2 mm. The laser beam was irradiated on the center of the C/SiC sample with a vertical angle of 90°. The main parameters of the laser device and hypersonic freestream are listed in Table 1 and Table 2, respectively. More details about the experimental setup, material preparation, laser device, hypersonic wind tunnel, characterization, can refer to our previous work [12].

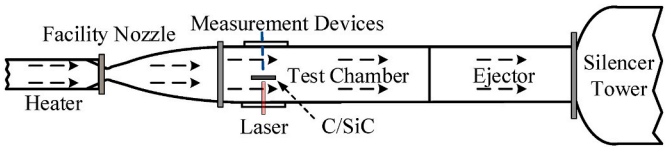

Fig. 1. Schematic of the laser ablation tests system in the hypersonic wind tunnel [12].

Table 1
Main parameters of the laser device in ablation test.

Parameters	Value
Laser wavelength (nm)	1070
Average laser power (W)	2000
Spot diameter (mm)	10
Laser power density(W/cm^2)	2546

Table 2
Main parameters of the hypersonic freestream in ablation test.

Parameters	Value
Total temperature (K)	1784
Static temperature (K)	222.4
Total pressure (kPa)	4257
Static pressure (kPa)	2.550
Mach number	6.0

As shown in Fig. 2, in order to reasonably reveal the acceleration mechanisms induced by the hypersonic airflow, three typical laser ablation tests of C/SiC composites in different conditions were conducted:

(1) *Test 1* was conducted in the static air condition, where the laser irradiated 4 s in the open static air environment;
(2) *Test 2* was conducted in the short-time hypersonic airflow condition, where both laser irradiation and tangential hypersonic airflow acted on the sample for 4 s;
(3) *Test 3* was conducted in the long-time hypersonic airflow condition, where the freestream firstly blew over the material surface for 60 s, and then the laser irradiated 5 s in the hypersonic airflow environment.

The comparison of *Test 1* and *Test 2* was conducted to investigate the influence induced by the hypersonic airflow, which mainly referred to the comprehensive effects of aerodynamic force and aerodynamic heat during the laser irradiation process. Moreover, considering that the hot

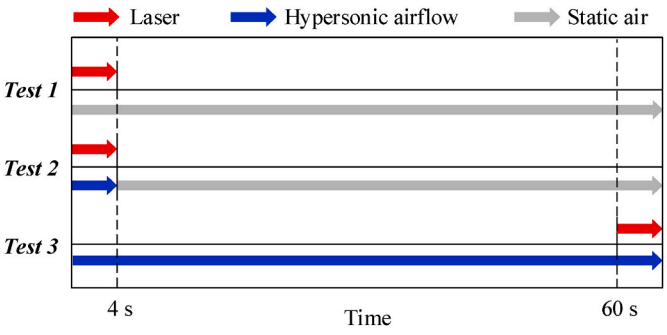

Fig. 2. The three laser ablation tests of C/SiC composite under different conditions.

structures of the hypersonic vehicles are typically in a state of thermal equilibrium due to the long-time aerodynamic heat, the comparison of *Test 2* and *Test 3* was further conducted to figure out the influence of aerodynamic heat effects before laser irradiation.

Detailed results of *Test 1* and *Test 2* can be found in Ref. [12], and *Test3* was additionally conducted in this paper. In *Test 3*, the stabilized freestream of Mach 6.0 blew over the material surface for 60 s before laser irradiation. Under this circumstance, the C/SiC composite was heated due to the aerodynamic heating effects, and reached the thermal equilibrium state.

Fig. 3 shows the profile of ablation pits along the central axis and ablation morphologies of C/SiC composites in different ablation tests. Generally, the laser ablated area of C/SiC composites can be divided into three regions: center, transition and edge region, due to the temperature variation from center to edge of ablation pit [12]. The ablation morphologies and mechanisms of the three regions were quite different [8, 12]. The sublimation of SiC matrix was adequate and partially sublimated carbon fibers were exposed at ablation center. The temperature of ablation transition region was lower and the ablation was dominated by the partial oxidation of the carbon fibers and the SiC matrix. At the ablation edge region, the liquid silicon oxide got solidified and deposited as a result of relatively low temperature. The mass and linear ablation rates of C/SiC in different test conditions were quantitatively contrasted in Fig. 4. Obviously, accelerated ablation phenomena can be observed. On the one hand, comparing *Test 1* and *Test 2*, it can be found that the mass and linear ablation rates increased by 413.2% and 51.8%, respectively. Thus, it is concluded that the laser ablation behavior was significantly multiplied by the combined effects of aerodynamic force and heat during the laser irradiation process. On the other hand, comparing *Test 2* and *Test 3*, it can be observed that the higher initial structure temperature condition caused by the aerodynamic heat would further increase the mass and linear ablation rates by 326.7% and 24.0%, respectively. Compared with the static air condition, mass ablation rate was augmented by 788.4% when the aerodynamic fully-heated sample was subjected to laser irradiation and hypersonic airflow. This accelerated ablation behavior was comparable to the "avalanche" phenomenon.

From the above, the "avalanche" phenomena of laser ablation under hypersonic airflow have been basically revealed through the proposed experimental studies. However, because of the strong coupling effects, experiments alone can hardly fully disclose the ablation mechanisms behind the phenomena, especially quantify the contributions of different aerodynamic effects (i.e. aerodynamic force, heat, gas concentration) on the different ablation mechanisms (i.e. oxidation, sublimation, mechanical erosion). Consequently, besides the experimental research, the coupled numerical analysis model was developed in the subsequent

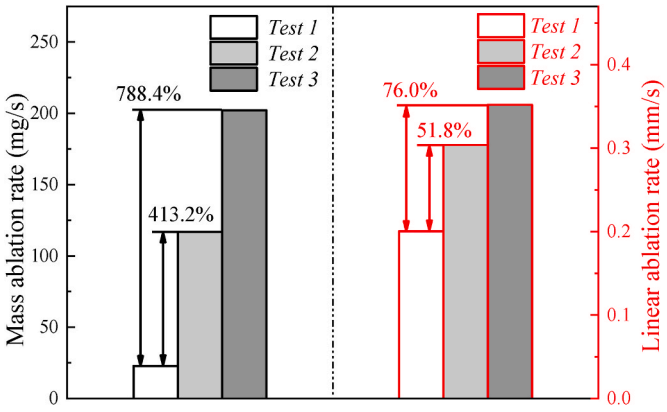

Fig. 4. Mass and linear ablation rates of C/SiC composites in different ablation tests.

section to further explore and decouple the mechanisms of "avalanche" phenomenon for laser ablation of C/SiC composites subjected to the hypersonic airflow.

3. Numerical models

The laser ablation behavior of C/SiC composites subjected to the hypersonic airflow is a typical fluid-thermal-ablation coupling issue. It involves two spatial domains (i.e. fluid domain and solid domain), and can be further separated into three distinct disciplines of aerothermodynamics in the fluid domain, and heat transfer as well as ablation in the solid domain. Each discipline is modeled individually and coupled at the fluid-solid interface by exchanging boundary information during the numerical simulation process.

3.1. Aerodynamic flow in fluid domain

The governing equations of the viscous compressible aerodynamic flow can be represented by the Favre-averaged Navier-Stokes (NS) equations, which can be written in integral form in Cartesian coordinates as follows:

$$\frac{\partial}{\partial t}\iiint_{\Omega}\mathbf{Q}\mathrm{d}V+\iint_{\partial\Omega}\left(\mathbf{F}_i^{\mathrm{c}}-\mathbf{F}_i^{\mathrm{v}}\right)n_i\mathrm{d}S=0\quad(i=1,2,3)\tag{1}$$

where Ω is the control volume, $\partial\Omega$ is the control volume boundary, $\mathrm{d}V$ is the volume integral element, $\mathrm{d}S$ is the surface integral element, n_i is the unit vector outward normal to $\mathrm{d}S$, $\mathbf{Q}$ is the state vector of conservative

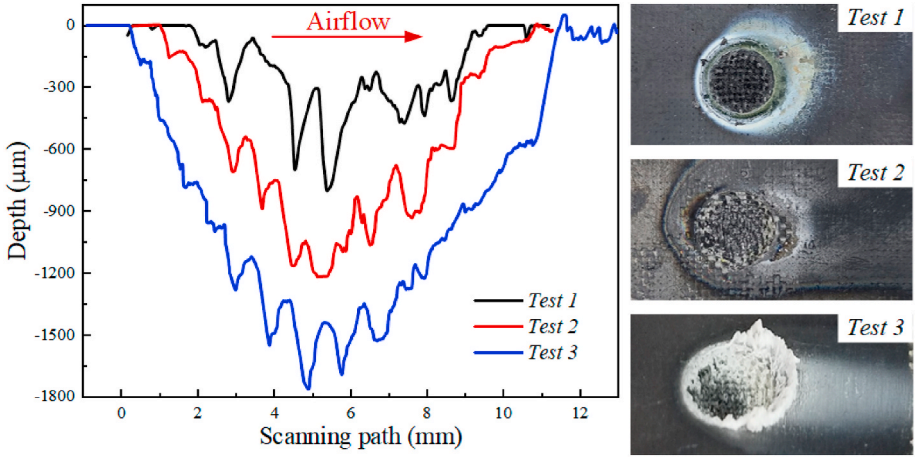

Fig. 3. Illustration of (a) profile of ablation pits along the central axis, and (b) ablation morphologies of 2D C/SiC composites in different ablation tests.

variables, $\mathbf{F}_i^c$ and $\mathbf{F}_i^v$ are the vectors of convective and viscous fluxes in the i-th coordinate direction, respectively.

In this paper, the aerodynamic characteristics were analyzed by the computational fluid dynamics (CFD) method. The Shear-Stress Transport (SST) k-ω model was adopted to characterize the turbulence. The second-order upwind scheme was utilized to spatially discretize the governing equations with the least squares cell-based gradient evaluation and the advection upstream splitting method (AUSM) flux-vector splitting. All the above equations were solved by ANSYS Fluent 16.0 [33].

3.2. Structural heat transfer in solid domain

According to the laws of energy conversation and Fourier heat conduction, the transient structural heat transfer can be expressed in Cartesian coordinates as follows:

$$\rho_s c_s \frac{\partial T_s}{\partial t} = \frac{\partial}{\partial x_i}\left(k_s \frac{\partial T_s}{\partial x_i}\right) + \dot{Q} + q_\Gamma \quad (i = 1, 2, 3) \tag{2}$$

where t is the time, T_s is the structural temperature, ρ_s is the density, c_s is the specific heat, k_s is the thermal conductivity, $\dot{Q}$ is the volumetric heating source in a solid, and q_Γ is the heat flux imposed on the boundary.

In this work, the structural heat transfer characteristics were analyzed by the computational solid dynamics (CSD) method. Eq. was discretized in spatial and time utilizing the finite element method (FEM) and implicit backward Euler method, respectively. And the Newton's method was adopted to solve the nonlinear equations.

3.3. Ablation recession in solid domain

In this section, the ablation recession model was established to capture the moving ablation surface. On the one hand, considering the surface chemical reaction kinetics, including the oxidation, and sublimation of SiC matrix and carbon fiber, the multi-component thermochemical ablation analysis model of C/SiC composites was established. On the other hand, considering the effect of airflow on mechanical erosion, the erosion model of C/SiC composites under thermomechanical loads was also constructed.

As shown in Fig. 5, the heterogeneous ablation of C/SiC composites occurred under high-speed airflow. On the composite surface, there appeared a boundary layer with ablation surface temperature T_w, airflow density ρ_e, pressure p_e, and surrounding speed u. All processes of chemical, heat and diffusive interaction were assumed to occur immediately on the interface of the composite and the boundary layer so that all characteristics of airflow did not change over the boundary layer thickness [12,15].

When the laser and airflow interact with composite, the ablation of materials was characterized by linear rate v, which motion along the normal to ablation surface. According to the models suggested in Ref. [13], the total rate v of C/SiC composite can be expressed as a linear superposition of three constituents:

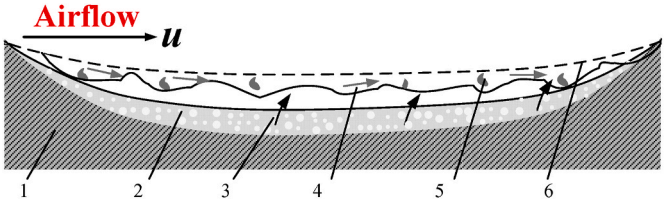

Fig. 5. Scheme of heterogeneous ablation of C/SiC composites under airflow: 1-initial composite, 2-pores in composite, 3- thermochemical ablation, 4-thermomechanical erosion. 5- ablation products. 6- boundary layer [12].

$$v = \frac{\dot{m}}{\rho_w} = v_o + v_s + v_e \tag{3}$$

where v_o, v_s, v_e denote the recession rates of chemical reaction of oxidization, sublimation, thermomechanical erosion under the high-speed overrunning hot flow of oxygen-containing gas, respectively; and ρ_w is the density on the ablation surface. Note that, for C/SiC composite, the internal erosion is ignored as no pyrolysis reaction occurs. Therefore, only the external erosion caused by the external hypersonic airflow should be considered.

The main work of the ablation model was to figure out the relationship between the degradation rate (v_o, v_s, v_e) and the airflow parameters (T_w, ρ_e, p_e, u).

3.3.1. Sublimation

Due to the high intensity of heat flux induced by CW laser, the temperature around the ablation center can reach high temperature (>3000 K) within a few seconds [8,12,34]. The sublimation of carbon fiber and SiC matrix inside composites occurred during the ablation progress. Moreover, at the high temperatures, sublimation of carbon will produce mostly C_3 [17,18]:

$$3C_{(s)} \rightarrow C_{3(g)} \tag{4}$$

$$SiC_{(s)} \rightarrow SiC_{(g)} \tag{5}$$

Then, the sublimation rate can be described by Dimitrienko's model [13]:

$$v_{s,i}(p_e, T_w) = \frac{1}{\rho_w}\left(h_c/C_p\right)\left(p_g^*/p_e\right)\exp\left(-\frac{E_{i,s}}{RT_w}\right) \tag{6}$$

where h_c is the convective heat transfer coefficient, C_p is the specific heat capacity at constant pressure, h_c/C_p is the heat transfer coefficient in the boundary layer, p_e is the local pressure of airflow, p_g^* is the constant characterizing a pressure of "initial state" of the generated gas phase, $E_{i,s}$ is the activation energy of the sublimation reaction, and R is the ideal gas constant (8.314 J/(mol•K)).

Thus, v_s can be expressed as the sum of the sublimation rates of fiber and matrix:

$$v_s = v_{s,C} + v_{s,SiC} \tag{7}$$

3.3.2. Oxidation

In this paper, only oxygen-induced oxidation reaction was considered. For the oxidation reaction of C/SiC (carbon and silicon carbide), it was controlled by the reactive regime and diffusive regime [35]. The oxidation regime was also affected by the surface temperature and concentration of oxygen, and there was a transition in the actual reaction process.

According to the Arrhenius thermochemical kinetic formula, the linear oxidation rate under kinetic reaction control mechanism can be described by Ref. [36]:

$$v_{o-reac,i} = \frac{\dot{m}_i}{\rho_w} = \frac{1}{\rho_w}\frac{aM_i}{M_{O_2}}A_{i,O}\exp\left(-\frac{E_{i,O}}{RT_w}\right)P_{Ow} \tag{8}$$

where a is the coefficient of the reaction equation, M_i is the molecular mass, M_{O2} is the relative molecular mass of oxygen, $E_{i,O}$ and A_i are the activation energy and pre-exponential factor respectively, P_{Ow} is the partial pressure of oxygen at ablation surface.

The ablation rate under diffusion control mechanism can be described by Ref. [36]:

$$v_{o-diff,i} = \frac{1}{\rho_w}\frac{h_c}{C_p}\frac{aM_i}{M_{O_2}}\omega_{O_2} \tag{9}$$

where h_c is the convective heat transfer coefficient, C_p is the specific heat

capacity at constant pressure, and a is the coefficient of the reaction equation, and ω_{O2} is the mass concentration of oxygen in the airflow.

When air flowing over the ablation surface, the oxidation rate was mainly related to the changing value of oxygen pressure P_{Ow}, mass concentration of oxygen ω_{O2}, convective heat transfer coefficient h_c, and surface temperature T_w. For C/SiC composites, the oxidation of carbon fiber and SiC matrix in oxygen was mainly considered [34]:

$$2C + O_2 = 2CO \tag{10}$$

$$2SiC + 3O_2 = 2SiO_2 + 2CO \tag{11}$$

$$SiC + O_2 = SiO + CO \tag{12}$$

Eq. is the oxidation of carbon fiber, Eq. and Eq. are the inert and active oxidation of SiC, respectively. For SiC, active oxidation will occur at low pressure and high temperature [37]. Therefore, the rection of SiC matrix was mainly dominated by active oxidation in this work.

Moreover, the actual oxidation rate should be the minimum of the rate under the reactive regime and diffusive regime [38]. The effect of temperature and pressure on chemical reaction control, and of oxidation concentration on diffusion control were both considered in the minimum control model:

$$v_o = \min\left(v_{o-reac}, v_{o-diff}\right) \tag{13}$$

3.3.3. Thermomechanical erosion

Thermomechanical erosion is a process of thermal ablation occurred on the surface of composite materials under the effect of high-speed airflow. For C/SiC composites, the internal pyrolysis can be ignored, so the main reason of erosion was that the external airflow overflows moving along the ablation surface of the composite [13].

The characteristics of thermomechanical erosion depended on the resistance properties, especially the strength of the composite that was corresponding to the direction of composites. Moreover, the erosion effect was also closely relating to the airflow, so the thermal erosion rate depended on the direction of materials and airflow. The linear rate of erosion v_e was the summarized rate of thermomechanical erosion of the composite, which was related to the external thermomechanical erosion rate of matrix v_m and fiber v_f.

The erosion rate of matrix and fiber was described in Ref. [12], and for transversally isotropic composites, there existed two different components about ablation rate of erosion [13,15]:

$$v_e = v_{e1}\left(n_1^2 + n_2^2\right) + v_{e2}n_3^2 \tag{14}$$

$$v_{e1} = \left(\frac{1-\delta_m}{v_{f\perp}} + \frac{\delta_m}{v_m}\right)^{-1} \tag{15}$$

$$\delta_m = h_m / \left(h_m + h_f\right) \tag{16}$$

$$v_{e2} = v_{f\parallel} \tag{17}$$

where v_{e1} is the rate of the surface orthogonal to the n_3 axis (thickness direction); v_{e2} is the rate of the surface orthogonal to the axis n_1 and n_2 (in-plane direction); $v_{f\perp}$ and $v_{f\parallel}$ are the rates of external thermomechanical erosion of fibers in transverse and longitudinal directions; δ_m is the relative thickness of the matrix interlayer between the layers of fibers in the unidirectional composite; h_m and h_f is the thicknesses of the layers of the matrix and fiber.

3.4. Energy and mass conservation in ablation surface

As Fig. 6 shows, energy conservation was followed on the ablation surface:

$$q_{in} = -\lambda\frac{\partial T}{\partial n} = q_{laser} - q_{rad} - q_{conv} - q_{phas} + q_{oxi} \tag{18}$$

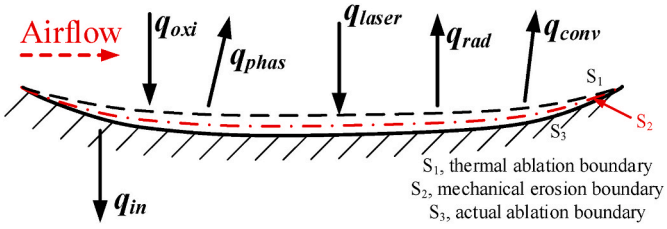

Fig. 6. Energy conservation on ablation surface of C/SiC composite.

where q_{laser} is the absorbed laser energy density; q_{rad} is the heat flux radiated from the ablation boundary to ambient airflow; q_{conv} is the convective heat transfer between the ablation boundary and ambient airflow; q_{phas} is the heat flux consumed by sublimation reaction; q_{oxi} is the heat flow released by the oxidation reaction; q_{in} is the heat flux transferred into the material.

The energy density caused by energy exchange can be described by:

$$q_{rad} = \sigma\varepsilon\left(T_w^4 - T_0^4\right) \tag{19}$$

$$q_{conv} = h_f\left(T_w - T_0\right) \tag{20}$$

The energy density caused by several ablation mechanisms can be separately described by the linear rate:

$$Q_{\text{phas}} = \sum m_i \int_{T_{-s}}^{T_s} c_i dT \tag{21}$$

$$q_{phas} = \frac{Q_{phas}\dot{m}_{phas}}{S} = Q_{phas}\rho_w\frac{dV_{phas}}{Sdt} = Q_{phas}\rho_w v_S \tag{22}$$

$$Q_{\text{oxi}} = C_{bef}\Delta H_{bef} - C_{aft}\Delta H_{aft} \tag{23}$$

$$q_{oxi} = \frac{Q_{oxi}\dot{m}_{oxi}}{S} = Q_{oxi}\rho_w\frac{dV_{oxi}}{Sdt} = Q_{oxi}\rho_w v_O \tag{24}$$

where Q_{phas} and Q_{oxi} are the reaction heat (endothermic or exothermic, J/kg) in sublimation and oxidation reaction, respectively.

In addition, mass conservation was also followed on the ablation surface:

$$\dot{m}_w = \dot{m}_{\text{chem}} + \dot{m}_{\text{ero}} - m_g \tag{25}$$

where $\dot{m}_w$ is the mass loss rate under ablation; $\dot{m}_{\text{chem}}$ is the mass loss rate caused by the chemical reaction; $\dot{m}_{\text{ero}}$ is the mass loss rate caused by the thermomechanical erosion, $\dot{m}_g$ is the consumed gas mass rate in the overrunning flow.

3.5. Numerical procedure

In the present paper, a loosely coupled fluid-thermal-ablation numerical method was proposed to predict the laser ablation behavior of C/SiC composites. The coupling algorithm is presented in Fig. 7, and the detailed implementation procedure can be summarized as follows:

(1) Construct individual discipline numerical analysis models. The numerical analysis models of high-speed fluid flow, structural heat transfer, structural ablation are firstly constructed.

(2) Conduct structural heat transfer analysis from t_i to t_{i+1}. The aerodynamic heat and ablation reaction heat on the coupling wall are interpolated from the fluid domain to the solid domain. Then, with the loads of aerodynamic heat, ablation reaction heat as well as laser heat, the transient structural heat transfer analysis from t_i to t_{i+1} can be accomplished. Especially, the aerodynamic heat and ablation reaction heat at the initial time are calculated with the initial structural temperature field.

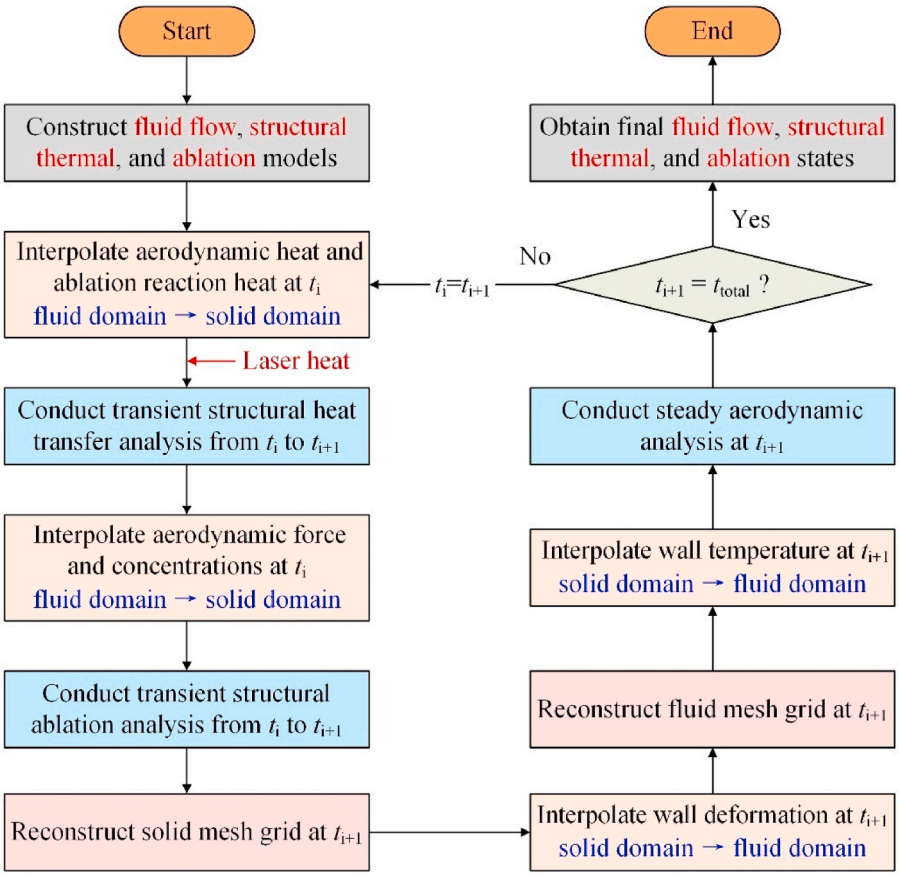

Fig. 7. Fluid-thermal-ablation coupling procedure.

(3) Conduct structural ablation analysis from t_i to t_{i+1}. The aerodynamic force and concentrations of gas components on the coupling wall are interpolated from the fluid domain to the solid domain. And then the transient structural ablation analysis from t_i to t_{i+1} can be conducted.

(4) Reconstruct both solid and fluid mesh grids. According to the structural deformation caused by the laser ablation, the solid mesh grid would be reconstructed. Subsequently, the deformation of the coupling wall is interpolated from the solid domain to the fluid domain. On this basis, the fluid mesh gird can be reconstructed.

(5) Conduct aerodynamic analysis from at t_{i+1}. The temperature of the coupling wall is firstly interpolated from the solid domain to the fluid domain. And then with the wall temperature condition, the steady aerodynamic analysis at t_{i+1} is performed.

(6) Check whether the total analysis time is reached. If the analysis time t_{i+1} reaches the total time t_{total}, end the coupled analysis, and the final states of fluid flow, structural thermal, and ablation can be obtained. Otherwise, update the analysis time from t_i to t_{i+1}, and then return to step (2).

(7) Loop. Repeating step (2) to step (5) until the total analysis time is reached.

Note that, to successfully carry out the above procedure, the data exchange method and mesh grid deformation method should be carefully considered. For the former, the hybrid interpolation strategy combining the inverse distance weighted (IDW) method and the radial basis function (RBF) method was adopted to transfer the coupling information [39], including aerodynamic heat, aerodynamic force, concentrations of gas components, structural temperature, structural deformation et al. As for the later, the Arbitrary Lagrange-Euler (ALE) algorithm [30,40], which was capable of maintaining a high-quality mesh by allowing the mesh to move independently of the material, was used to reconstruct the internal grids of the solid and fluid domains.

3.6. Case study

In this section, the ablation behavior of 2D C/SiC plane subjected to hypersonic airflow and laser irradiation was numerically analyzed. As illustrated in Fig. 8, a three-dimensional simulation model has been developed to reproduce the experimental tests. Especially, because of the symmetry, only one-half model was considered to improve the computational efficiency.

Obviously, the computational domain was divided into two zones:

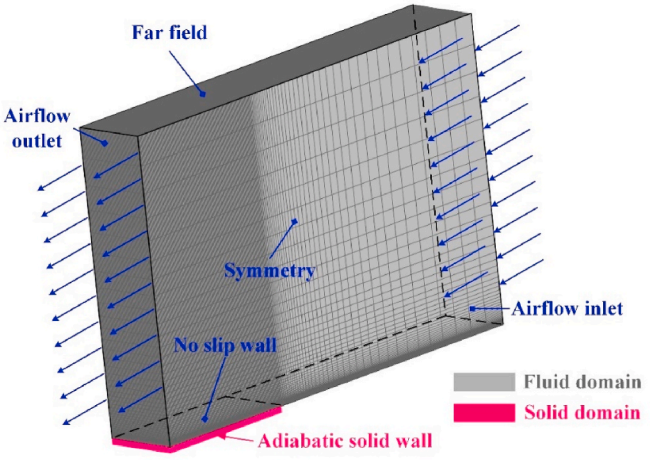

Fig. 8. Illustration of three-dimensional simulation model.

fluid domain and solid domain. For the fluid domain, the overall size was 150mm × 100mm × 25 mm, and the CFD grid was constructed with a structural gird of 150 × 81 × 76 nodes. The grid near the wall was refined to 1×10^{-3} mm in the normal direction and 2×10^{-1} mm in the streamline direction to accurately capture the near wall phenomena. The CFD model was constrained to three boundary conditions, namely, hypersonic airflow inlet, far field, outlet, no slip wall and symmetry. For the solid domain, the overall size of the 2D C/SiC plate was 50mm × 25mm × 2 mm, and the CSD grid was constructed with a structured grid of 101 × 51 × 10 nodes. The grid near the laser irradiation region was refined to 2×10^{-1} mm to accurately obtain the ablation morphology. For the boundary conditions, heat flux was prescribed on the coupling surface of the C/SiC plate, while the other surfaces were assumed perfectly insulated. Additionally, the material properties of the 2D C/SiC composites (40% carbon fiber, 42.2% SiC matrix) and the ablation formulation parameters can be listed in Table 3 [9,41].

The energy density of CW laser was not sufficient for photoionization or thermal ionization [42], therefore the plasma screening effect was neglected in this paper. When a laser irradiates the target surface, the laser energy deposition in the C/SiC composites can be estimated according to the Lambert-Beer-Bouguer law [43]:

$$q = (1 - R) q_{inc} e^{-\alpha(T) z} \tag{26}$$

where q is the value of laser power density at depth z, R is the reflectivity of material, $\alpha(T)$ is the optical absorption coefficient of the material, q_{inc} is the laser power density irradiated on the material surface.

In preparation of the composite samples, C/SiC surface was coated by SiC layer and carbon fibers were covered with SiC matrix. In previous work, the SiC absorption coefficient of near-infrared laser radiation was studied at high temperatures, and the analysis focused on the spectral range of 1070 nm [44], which was identical to the laser wavelength in our work. The optical absorption coefficient α started at 1×10^4 m^{-1} at 1000 K, and revealed a significant increase at rising temperature during the ablation, indicating a greater value of α. Therefore, the volume absorption can be neglected, and the laser absorption of C/SiC can be simplified as surface absorption. And Eq. can be rewritten as

$$q = (1 - R) q_{inc} \tag{27}$$

Moreover, the reflectivity properties and energy deposition were complicated with the ablation progress. Indeed, the reflectivity properties will change during ablation, which is related to surface temperature, phase transition and surface roughness [45], etc. Some published works have studied the optical properties (reflectivity properties under radiation) of multiple carbon fiber, SiC and ceramic matrix composites at the wavelength of 1070 nm [46–48]. According to these researches, the reflectivity was around 0.2 and it changed little with temperature. Thus, the reflectivity of the C/SiC to laser was properly set to 0.2 in the numerical analysis model.

Table 3
Material properties and ablation formulation parameters of the 2D C/SiC composite.

Parameters	Value	Unit
ρ_w	2050	kg/m^3
ρ_f	1760	kg/m^3
ρ_m	3190	kg/m^3
k_f	42	W/(m·K)
k_m	20	W/(m·K)
c_f	600	J/(kg·K)
c_m	700	J/(kg·K)
$E_{C,\,S}$	6.65×10^5	J/mol
$E_{SiC,\,S}$	8.73×10^4	J/mol
M_{O2}	32	–
M_C	12	–
M_{SiC}	40	–
$A_{C,O}$	5.77×10^5	kg/m^3•s
$A_{SiC,O}$	10	kg/m^3•s
$E_{C,O}$	1.142×10^5	J/mol
$E_{SiC,O}$	9.46×10^4	J/mol
J_f^0	5.4×10^2	kg/m^3•s
J_m^0	5×10^5	kg/m^3•s
$\sigma_{f\parallel}/\sigma_{f\perp}$	2200/220	MPa
σ_m	400	MPa
E_{Af}	5.4×10^4	J/mol
E_{Am}	8.73×10^4	J/mol

4. Results and discussions

4.1. Comparison of the experimental and numerical results

According to the experimental tests in Section 2, three numerical cases were correspondingly conducted in this section:

(1) *Case 1*: Ablation behaviors in static air (corresponding to *test 1*);
(2) *Case 2*: Ablation behaviors in short-time hypersonic airflow (corresponding to *test 2*);
(3) *Case 3*: Ablation behaviors in long-time hypersonic airflow (corresponding to *test 3*).

To demonstrate the established numerical model, Fig. 9 gives the comparison of experimental and numerical results on the temperature histories at the center of the back-surface over ablation time. We can see that the numerical results had the similar tendency to the experimental results, and the maximum errors of the temperature were 17.2% and 12.2% in *Case 1* and *Case 2*, respectively. Moreover, Fig. 10 (a1), (a2), (a3) show the numerical ablation profiles evolution of three ablation cases over ablation time. Compared with the ablation results in *Case 1*, the ablation depth in *Case 2* increased greatly, and the ablation pit in *Case 3* further appeared with greater depth and width. Fig. 10 (b) further gives the comparison of experimental and numerical results on the final ablation profiles. Qualitatively, it can be observed that the numerical results had a good agreement with the experimental data on the shape of the ablation profile. Quantitatively, the depth of ablation center appeared 0.693 mm, 1.035 mm and 1.518 mm in the experimental *Test 1*, *Test 2* and *Test 3*, respectively. The corresponding data was 0.577 mm, 1.153 mm and 1.734 mm in the numerical *Case 1*, *Case 2* and *Case 3*, respectively. The errors of experimental and numerical results were 16.8%, 11.4% and 14.2%, respectively. The possible reasons involved the measured error and material dispersion in the experimental test, as well as the ablation model error in the numerical analysis. Notwithstanding, considering the complexity of the multi-field coupling problem, these results suggested that the proposed analysis model was

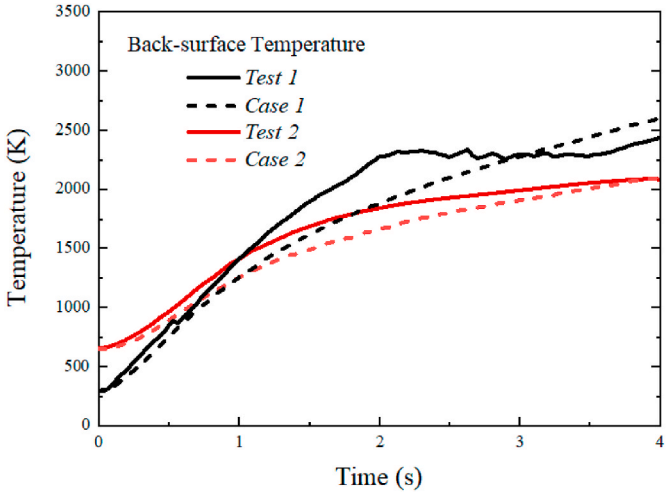

Fig. 9. Comparison of experimental and numerical results on the temperature histories at the center of back surface.

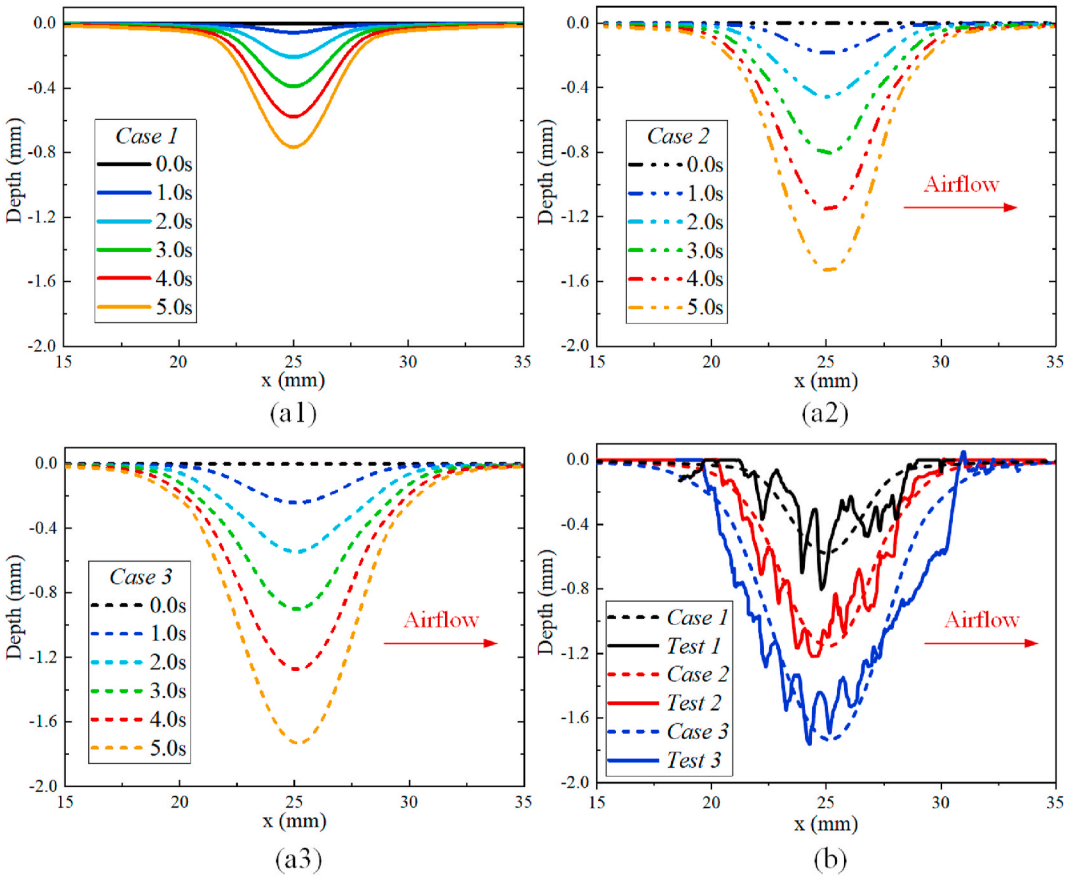

Fig. 10. The numerical ablation profiles evolution of (a1) *Case 1*, (a2) *Case 2*, (a3) *Case 3* over ablation time, and (b) comparison of experimental and numerical results on the final ablation profiles.

reliable to predict the laser ablation behaviors of C/SiC composite subjected to high-speed airflow.

4.2. Effects of hypersonic airflow on ablation behaviors

To explore the influence of the hypersonic airflow on the laser ablation behavior, the contrast study between *Case 1* and *Case 2* was carefully conducted. Fig. 11 shows the comparisons on the temperature history and the ablation rates of different ablation mechanisms at the ablation center of C/SiC composites. According to the temperature

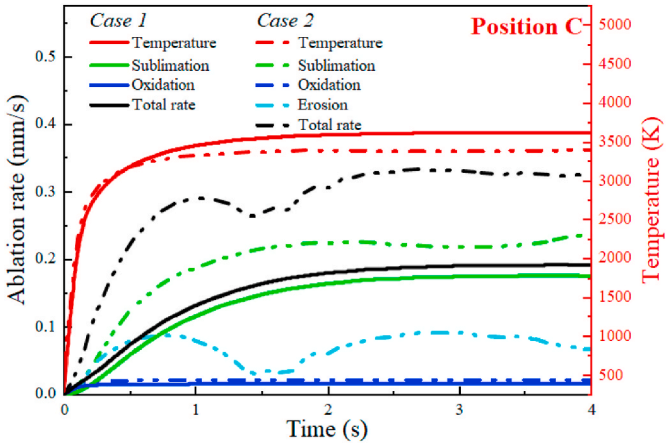

Fig. 11. Ablation rates, temperature history at ablation center for *Case 1* and *Case 2*.

history of *Case 2*, the wall temperature increased to 1784 K (the total temperature of the incoming airflow) within a very short time (t = 0.07s), which indicated that the aerodynamic heating changed from the aerodynamic heating effect to the aerodynamic cooling effect soon after the ablation began, thus the coupling wall temperature in *Case 2* was lower than that in *Case 1*. This phenomenon was also reported in our previous work [12].

Moreover, for both *Case 1* and *Case 2*, the oxidation rate first increased below the temperature of 2500 K under reactive regime, and then stabilized at a constant level at higher temperatures due to the stable diffusion rate of oxidizers to the ablation surface under diffusive regime. The oxidation rate in *Case 2* slightly increased as a result of the accelerated diffusion under the high-speed airflow. For the sublimation reaction, owing to the extra high temperature (>3500 K) at ablation center, the sublimation effect was the dominant ablation mechanism in the static environment (*Case 1*). Compared with *Case 1*, although the temperature of the ablation center was relatively low, a decreased static pressure would lead to a higher sublimation rate in the hypersonic airflow (*Case 2*), and sublimation still dominated the ablation progress. In addition, the ablation recession induced by erosion effect occurred under the hypersonic airflow, which caused a further increase in total ablation rate. Through the time integration of the ablation rate over the whole process (4 s), the total ablation depth contributions of sublimation, oxidation and erosion accounted for 89.93%, 10.07% and 0% in *Case 1*, while 68.06%, 7.43% and 24.51% in *Case 2*.

In general, sublimation effect dominated at ablation center in both the static air and hypersonic airflow environment, but the total rate under hypersonic airflow sharply increased due to the enhancement of sublimation effect and extra erosion effect.

4.3. Effects of aerodynamic heat on laser ablation behaviors

As mentioned before, the difference on the aerodynamic heat effect before laser irradiation between *Case 2* and *Case 3* caused different initial structural temperature distributions, which would further lead to different laser ablation behaviors. Thus, the comparison of *Case 2* and *Case 3* on the aerodynamic characteristics and ablation rate was conducted to figure out the influence of aerodynamic heat effects.

4.3.1. Aerodynamic characteristics

The ablation behaviors were closely related to aerodynamic characteristics around the ablation surface, which was varying with time and space. Fig. 12 gives the time evolution of pressure distribution on the coupling wall in *Case 2* and *Case 3*. Similar pressure evolutions were found, the local pressure and pressure head both appeared maximum at downstream area. But there were differences in values for the two cases, and *Case 3* appeared higher pressure head and lower local pressure.

For the further analysis of the relation between aerodynamic characteristics and ablation profile, five typical positions inside the ablation pit, i.e., upstream area (A, B), center (C), downstream area (D, E), were taken for analysis. The time evolutions of local pressure on the five positions in *Case 2* and *Case 3* are given in Fig. 13 (a). It can be found that the local pressure was varying over ablation time due to the change of the ablation pit over the ablation process. And the local pressure on the specific positions in *Case 2* and *Case 3* showed similar tendencies: (1) it decreased at upstream and center area (position A, B, C) because the high-speed airflow was expanded over the convex ablation wall; (2) it got increased at downstream area (position D, E) on account of the airflow compression over the concave ablation wall.

Meanwhile, for both *Case 2* and *Case 3*, due to the greatly varied velocity gradient of the boundary layer near the ablation surface, the pressure head presented significant differences along the ablation pit, as shown in Fig. 13 (b). At the same depth, the pressure head on the downstream area (position E, D) was higher than that at upstream area (position A, B). And the pressure head would decrease to the smallest degree on the ablation center (position C) as the air velocity decreased rapidly at the deep area of the ablation pit. Additionally, owing to the greater ablation temperature and ablation depth, *Case 3* appeared higher pressure head and lower local pressure compared to *Case 2*, which led to greater erosion and sublimation effect in *Case 3*.

4.3.2. Decoupling ablation mechanisms

The influence of hypersonic airflow on laser ablation rate was further examined. Figs. 14–16 illustrate the temperature history and ablation rates contributed by various mechanisms of positions A-E in *Case 2* and *Case 3*. Overall, there was little difference in oxidation rates between the two cases, whereas both the sublimation rates and the erosion rates were increased in *Case 3*, resulting in a higher total rate of linear ablation.

The same as mentioned in Section 4.3, the oxidation rate first increased under reactive regime and then stabilized at a constant level under diffusive regime, and remained almost equal in *Case 2* and *Case 3* with the same airflow condition. The recession rate of sublimation and erosion mainly varied corresponding to the local pressure and pressure head, respectively. The ablation mechanisms contributions of specific positions in *Case 2* and *Case 3* shared similar tendencies, but *Case 3* appeared greater ablation rate due to higher temperature, lower local pressure and higher pressure head. For all the positions in the two cases, the erosion rate appeared a similar trend: it first increased as temperature rising, then decreased due to the sharp drop of the pressure head, but rose again after a specific transition moment. These transition moments are marked in Figs. 14–16, respectively. The ablation depth at the transition moments of different positions was consistent, with a depth at approximately 0.367 mm. This finding may be related to the flow pattern transition as the evolution of ablation pits [49].

Besides, the ablation mechanisms contributions were contrasted for the position A and E (also B and D), which had the same depth and close temperature history under ablation. As shown in Fig. 14, for position A, the total ablation depth contributions of sublimation, oxidation, erosion accounted for 42.68%, 17.88%, 39.44% in *Case 2*, and 48.63%, 13.49%, 37.88% in *Case 3*. For position E, the total ablation depth contributions were changed to 34.11%, 17.44%, 48.45% in *Case 2*, and 41.28%, 13.25%, 45.47% in *Case 3*. It can be observed that sublimation and erosion dominated the ablation process, and compared with position A, the contribution of erosion effect at position E increased as a result of

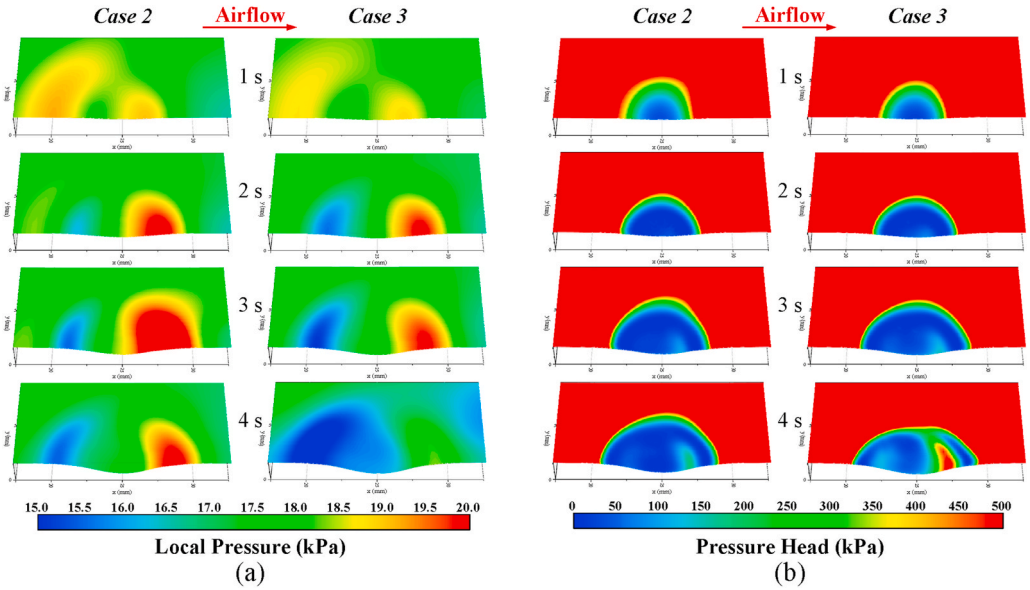

Fig. 12. Time evolution of pressure distribution on the coupling wall in *Case 2* and *Case 3* (one-half model): (a) local pressure; (b) pressure head.

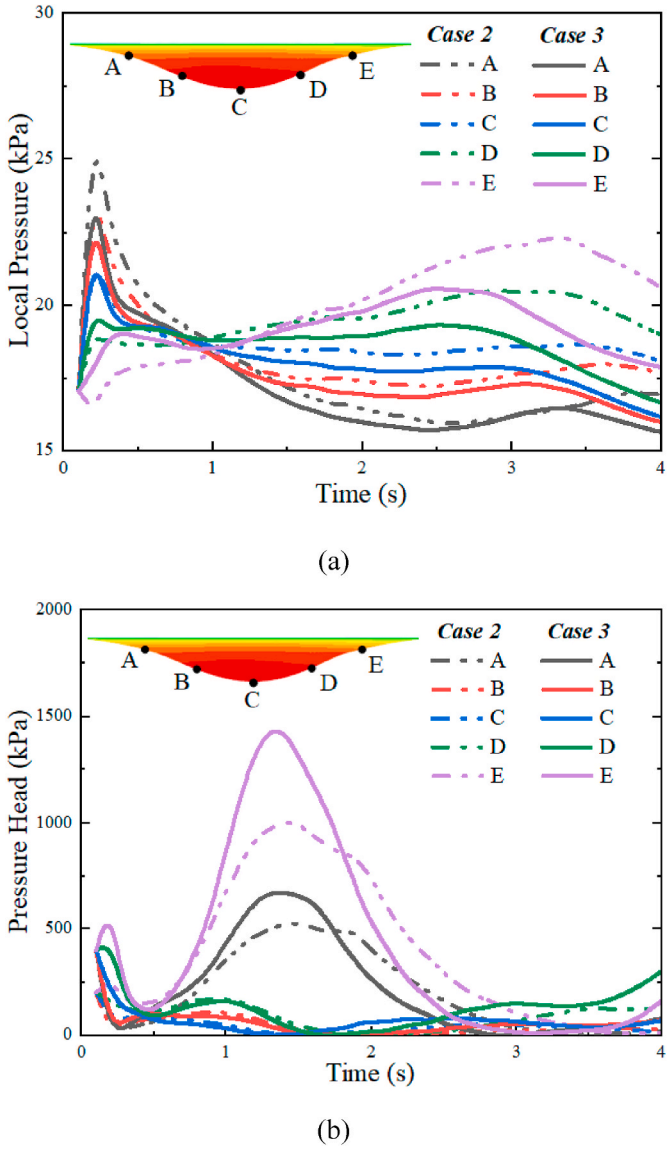

Fig. 13. Pressure distribution of five positions in ablation pit for *Case 2* and *Case 3*: (a) local pressure; (b) pressure head.

higher pressure head at downstream area.

Additionally, as shown in Fig. 15, for position B, the total ablation depth contributions were 65.42%, 9.61%, 24.97% in *Case 2*, and 67.32%, 7.53%, 25.15% in *Case 3*. For position D, it was changed to 58.64%, 9.39%, 31.96% in *Case 2*, and 60.17%, 7.23%, 32.60% in *Case 3*. Compared with positions A and E, the contribution of erosion effect was augmented at positions B and D, which was caused by the much higher temperature at downstream area. And compared with position B, the rise of erosion proportion was more obvious at position D after 2.0 s, and the erosion rate reached to 0.140 mm/s and 0.101 mm/s at 4.0s in *Case 2* and *Case 3*, which were maximum of all positions.

For position C (ablation center) shown in Fig. 16, the total ablation depth contributions of sublimation, oxidation and erosion accounted for 68.06%, 7.43%, 24.51% in *Case 2*, and 69.24%, 5.89%, 24.87% in *Case 3*. Compared with the other positions, the erosion effect decreased to the lowest level while the sublimation effect increased to the highest level in position C due to the small pressure head and highest surface temperature. Under the circumstances, the sublimation reaction played a leading role in ablation process, and the sublimation rate reached to 0.302 mm/s and 0.239 mm/s at 4.0s in *Case 2* and *Case 3*, which were the maximum of all positions.

Moreover, compared with *Case 2*, greater sublimation and erosion rates occurred in *Case 3* owing to lower local pressure (Fig. 13 (a)), higher pressure head (Fig. 13 (b)), and higher temperature (Figs. 14, Fig. 15, Fig. 16), which were caused by the greater aerodynamic heat effect. Take the ablation center for example, the ablation depth contributed by sublimation effect was 0.767 mm in *Case 2*, while 0.912 mm in *Case 3*. Additionally, the ablation depth contributed by erosion effect was 0.276 mm in *Case 2*, while 0.328 mm in *Case 3*. Thus, the increased sublimation and erosion rates caused more ablation depth in *Case 3*, which reflected that the aerodynamic heat effect was also one of the key reasons for the "avalanche" phenomenon, in addition to the reason mentioned in Section 4.2. Therefore, it can be concluded that the total ablation rate would be greatly augmented in the hypersonic airflow environment, especially under a long-time loading of aerodynamic heat before laser irradiation.

5. Conclusions

In this paper, the significantly accelerated laser ablation phenomena ("avalanche" phenomenon) for C/SiC composites under hypersonic airflow were discovered. To reveal the mechanisms of the "avalanche" phenomenon, several parallel experiments were carried out, and coupled fluid-thermal-ablation numerical simulations were performed. The relationship between ablation rates and aerodynamic effects was discussed, and contributions of each ablation mechanism to the total ablation behavior were quantitively evaluated. The main conclusions are summarized as follows:

(1) In the open static air environment, the sublimation effect dominated the laser ablation progress, as a result of extra high temperature at ablation region.
(2) Compared with the ablation rate in the static air environment, the ablation rate in the short-time hypersonic airflow environment

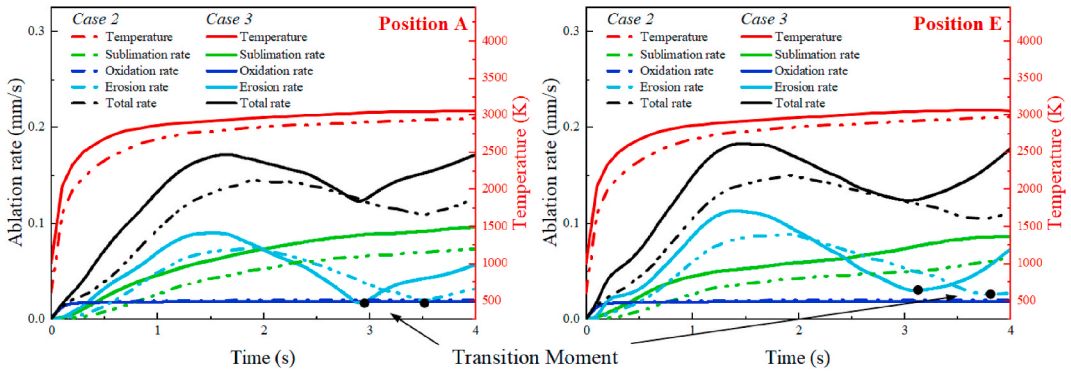

Fig. 14. Ablation rates, temperature history of position A and E for *Case 2* and *Case 3*.

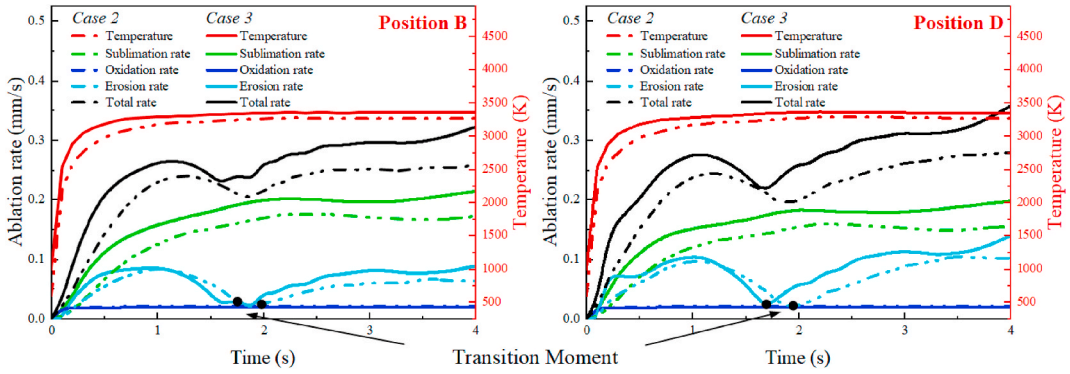

Fig. 15. Ablation rates, temperature history of position B and D for *Case 2* and *Case 3*.

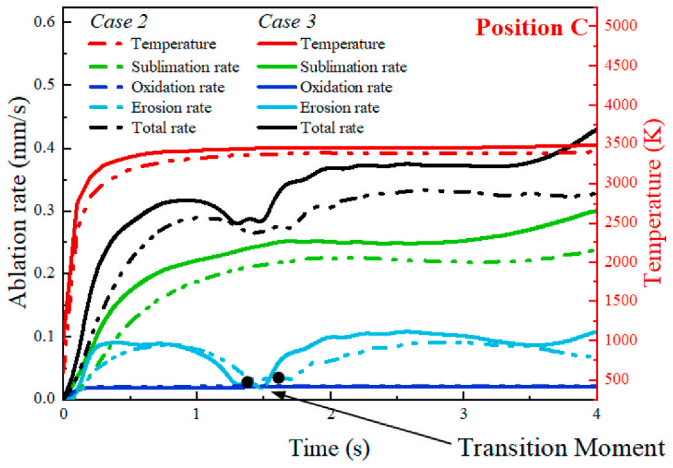

Fig. 16. Ablation rates, temperature history of position C for *Case 2* and *Case 3*.

sharply increased due to the enhancement of sublimation effect and extra erosion effect, which were caused by the decreased local pressure and increased pressure head, respectively.

(3) Moreover, compared with the ablation rate in the short-time hypersonic airflow, the ablation rate in the long-time hypersonic airflow condition further increased due to the enhancement of sublimation and erosion effects, the main causes of which were the higher temperature, lower local pressure and higher pressure head induced by the long-time aerodynamic heat effect before the laser irradiation.

Generally, the combined effect of augmented sublimation and accelerated erosion accounted for the main reasons of "avalanche" phenomenon for the laser behavior of C/SiC composite under hypersonic airflow, and the aerodynamic heat effect would further intensify this phenomenon.

Declaration of competing interest

The authors declare that they have no known competing financial interests or personal relationships that could have appeared to influence the work reported in this paper.

Data availability

Data will be made available on request.

Acknowledgements

Financial supports from the National Natural Science Foundation of China (Grant Nos. 11902322, 11472276, 11332011, 11972035, 91016025 and 11972033), and Strategic Priority Research Program of the Chinese Academy of Sciences (Grant No. XDA22000000), are gratefully acknowledged.

References

[1] S. Schmidt, S. Beyer, H. Knabe, H. Immich, R. Meistring, A. Gessler, Advanced ceramic matrix composite materials for current and future propulsion technology applications, Acta Astronaut. 55 (2004) 409–420.
[2] D. Glass, Ceramic matrix composite (CMC) thermal protection systems (TPS) and hot structures for hypersonic vehicles, in: 15th AIAA Int. Sp. Planes Hypersonic Syst, Technol. Conf., 2008, p. 2682.
[3] L. Zhang, L. Cheng, X. Luan, H. Mei, Y. Xu, Environmental performance testing system for thermostructure materials applied in aeroengines, Key Eng. Mater. 313 (2006) 180–183.
[4] L. Long, Y. Huang, J. Zhang, Experimental investigation and numerical simulation on continuous wave laser ablation of multilayer carbon fiber composite, Proc. Inst. Mech. Eng. Part L J. Mater. Des. Appl. 231 (2015).
[5] P. Nan, Z. Shen, B. Han, X. Ni, The influences of laminated structure on the ablation characteristics of carbon fiber composites under CW laser irradiation, Opt Laser. Technol. 116 (2019) 224–231.
[6] J. Wang, W. Yuan, Y. Liu, H. Song, C. Huang, High-power laser resistance of filled sandwich panel with truss cores: ablation mechanisms and numerical simulation, Compos. Struct. 203 (2018) 574–584.
[7] B. Sinkovics, P. Gordon, G. Harsányi, Computer modelling of the laser ablation of polymers, Appl. Therm. Eng. 30 (2010) 2492–2498.
[8] Y. Tong, S. Bai, H. Zhang, Y. Ye, Laser ablation behavior and mechanism of C/SiC composite, Ceram. Int. 39 (2013) 6813–6820.
[9] X. Dang, X. Yin, X. Fan, Y. Ma, J. Wang, P. Ju, H. Song, Microstructural evolution of carbon fiber reinforced SiC-based matrix composites during laser ablation process, J. Mater. Sci. Technol. 35 (2019) 2919–2925.
[10] M. Su, L. Cheng, X. Luan, L. Zhang, Laser ablation behaviors of C/SiC composites in air, Acta Mater. Compos. Sin. (2013) 37–47.
[11] J. Wang, Y. Ma, Y. Liu, W. Yuan, H. Song, C. Huang, X. Yin, Experimental investigation on laser ablation of C/SiC composites subjected to supersonic airflow, Opt Laser. Technol. 113 (2019) 399–406.
[12] Z. Wang, J. Wang, H. Song, W. Yuan, Y. Liu, T. Ma, C. Huang, Laser ablation behavior of C/SiC composites subjected to transverse hypersonic airflow, Corrosion Sci. 183 (2021) 109345.
[13] Y.I. Dimitrienko, Thermomechanics of Composite Structures under High Temperatures, Thermomechanics of Composite Structures under High Temperatures, 2016.
[14] Y.I. Dimitrienko, Modeling of erosion combustion of energetic materials in high-enthalpy flows, Combust. Flame 111 (1997) 161–174.
[15] Y.I. Dimitrienko, I.D. Dimitrienko, Effect of thermomechanical erosion on heterogeneous combustion of composite materials in high-speed flows, Combust. Flame 122 (2000) 211–226.
[16] C. Park, Stagnation-point ablation of carbonaceous flat disks. I Theory, AIAA J. 21 (11) (1983) 1588–1594.
[17] C. Park, Calculation of stagnation-point heating rates associated with stardust vehicle, J. Spacecraft Rockets 44 (2007) 24–32.
[18] Y.K. Chen, F.S. Milos, Navier-Stokes solutions with finite rate ablation for planetary mission earth reentries, J. Spacecraft Rockets 42 (2005) 961–970.
[19] Y. Wang, C.L. Pasiliao, Modeling ablation of laminated composites: a novel manual mesh moving finite element analysis procedure with ABAQUS, Int. J. Heat Mass Tran. 116 (2018) 306–313.

[20] W. Li, H. Huang, X. Xu, A coupled thermal/fluid/chemical/ablation method on surface ablation of charring composites, Int. J. Heat Mass Tran. 109 (2017) 725–736.
[21] W. Li, H. Huang, Q. Wang, Z. Zhang, Protection of pyrolysis gases combustion against charring materials' surface ablation, Int. J. Heat Mass Tran. 102 (2016) 10–17.
[22] W. Li, H. Huang, X. Xu, J. Guo, A new mechanism of surface ablation of charring materials for a vehicle during reentry, Appl. Therm. Eng. 106 (2016) 838–849.
[23] W. Li, H. Huang, B. Ai, Z. Zhang, On the novel designs of charring composites for thermal protection application in reentry vehicles, Appl. Therm. Eng. 93 (2016) 849–855.
[24] W. Li, H. Huang, Y. Tian, Z. Zhao, A nonlinear pyrolysis layer model for analyzing thermal behavior ofcharring ablator, Int. J. Therm. Sci. 98 (2015) 104–112.
[25] F. Ren, H.S. Sun, L.Y. Liu, Theoretical analysis for mechanical erosion of carbon-base materials in ablation, J. Thermophys. Heat Tran. 10 (1996) 593–597.
[26] B.W. Barr, Investigation and Modeling of Coupled Thermochemical and Thermomechanical Erosion in Thermally Degrading Systems, 2012.
[27] X. Luan, L. Cheng, C. Xie, Stressed oxidation life predication of 3D C/SiC composites in a combustion wind tunnel, Compos. Sci. Technol. 88 (2013) 178–183.
[28] D. Bianchi, F. Nasuti, E. Martelli, Navier-Stokes simulations of hypersonic flows with coupled graphite ablation, J. Spacecraft Rockets 47 (2010) 554–562.
[29] A. Martin, I.D. Boyd, Strongly coupled computation of material response and nonequilibrium flow for hypersonic ablation, J. Spacecraft Rockets 52 (2015) 89–104.
[30] S. Meng, Y. Zhou, W. Xie, F. Yi, S. Du, Multiphysics coupled fluid/thermal/ablation simulation of carbon/carbon composites, J. Spacecraft Rockets 53 (2016) 930–935.
[31] P. Schrooyen, A. Turchi, K. Hillewaert, P. Chatelain, T.E. Magin, Two-way coupled simulations of stagnation-point ablation with transient material response, Int. J. Therm. Sci. 134 (2018) 639–652.
[32] A. Turchi, P.M. Congedo, T.E. Magin, Thermochemical ablation modeling forward uncertainty analysis—Part I: numerical methods and effect of model parameters, Int. J. Therm. Sci. 118 (2017) 497–509.
[33] ANSYS, ANSYS Fluent 16.0 Theory Guide, 2015.
[34] Z. Chen, D. Fang, Y. Miao, B. Yan, Comparison of morphology and microstructure of ablation centre of C/SiC composites by oxy-acetylene torch at 2900 and 3550° C, Corrosion Sci. 50 (2008) 3378–3381.
[35] J. Lachaud, Y. Aspa, G.L. Vignoles, Analytical modeling of the transient ablation of a 3D C/C composite, Int. J. Heat Mass Tran. 115 (2017) 1150–1165.
[36] H. Huang, X. Xu, G. Jiang, Discrimination for ablative control mechanism in solid-propellant rocket nozzle, Sci. China Ser. E Technol. Sci. 52 (2009) 2911–2917.
[37] W.L. Vaughn, H.G. Maahs, Active-to-passive transition in the oxidation of silicon carbide and silicon nitride in air, J. Am. Ceram. Soc. 73 (1990) 1540–1543.
[38] B. Zhang, Y. Liu, C. Wang, J. Ren, New discrimination method for ablative control mechanism in solid-propellant rocket nozzle, Sci. China Technol. Sci. 53 (2010) 2718–2724.
[39] F. Chen, H. Liu, S. Zhang, Coupled heat transfer and thermo-mechanical behavior of hypersonic cylindrical leading edges, Int. J. Heat Mass Tran. 122 (2018) 846–862.
[40] ABAQUS Documentation, Version 6.13, Dassault Systèmes Simulia Corp., Providence, RI, USA, 2014.
[41] Y. Xu, S. Ren, W. Zhang, Thermal conductivities of plain woven C/SiC composite: micromechanical model considering PyC interphase thermal conductance and manufacture-induced voids, Compos. Struct. 193 (2018) 212–223.
[42] J. Ready, Effects of High-Power Laser Radiation, Elsevier, 2012.
[43] L. Li, D. Zhang, Z. Li, L. Guan, X. Tan, R. Fang, D. Hu, G. Liu, The investigation of optical characteristics of metal target in high power laser ablation, Phys. B Condens. Matter 383 (2006) 194–201.
[44] B. Adelmann, R. Hellmann, SiC absorption of near-infrared laser radiation at high temperatures, Appl. Phys. A 122 (2016) 642.
[45] S. Pan, Q. Li, Z. Xian, N. Su, F. Zeng, The effects of laser parameters and the ablation mechanism in laser ablation of C/SiC composite, Materials 12 (2019) 3076.
[46] C. Freitag, R. Weber, T. Graf, Polarization dependence of laser interaction with carbon fibers and CFRP, Opt Express 22 (2014) 1474–1479.
[47] H. Aréna, M. Coulibaly, A. Soum-Glaude, A. Jonchère, G. Arrachart, A. Mesbah, N. Pradeilles, M. Vandenhende, A. Maître, X. Deschanels, Effect of TiC incorporation on the optical properties and oxidation resistance of SiC ceramics, Sol. Energy Mater. Sol. Cells 213 (2020) 110536.
[48] R. Brandt, M. Frieß, G. Neuer, Thermal conductivity, specific heat capacity, and emissivity of ceramic matrix composites at high temperatures, High. Temp. - High. Press. 35 (2003) 169–177.
[49] Y. Huang, H. Song, C. Huang, Heat transfer and mode transition for laser ablation subjected to supersonic airflow, Chin. Phys. Lett. 33 (2016) 14201.